Formation of Stacking Faults and the Screw Dislocation-Driven Growth: A Case Study of Aluminum Nitride Nanowires

Fei Meng,[†] Marc Estruga,[†] Audrey Forticaux,[†] Stephen A. Morin,[§] Qiang Wu,[‡] Zheng Hu,[‡] and Song Jin[†,*]

[†]Department of Chemistry, University of Wisconsin-Madison, 1101 University Avenue, Madison, Wisconsin 53706, United States and [‡]Key Lab of Mesoscopic Chemistry of MOE and Jiangsu Provincial Laboratory for NanoTechnology, Department of Chemistry, Nanjing University, Nanjing 210093, China. [§]Present address: Department of Chemistry, University of Nebraska-Lincoln, Lincoln, Nebraska 68588, United States.

ABSTRACT Stacking faults are an important class of crystal defects commonly observed in nanostructures of close packed crystal structures. They can bridge the transition between hexagonal wurtzite (WZ) and cubic zinc blende (ZB) phases, with the most known example represented by the "nanowire (NW) twinning superlattice". Understanding the formation mechanisms of stacking faults is crucial to better control them and thus enhance the capability of tailoring physical properties of nanomaterials through defect engineering. Here we provide a different perspective to the formation of stacking faults associated with the screw dislocation-driven growth mechanism of nanomaterials. With the use of NWs of WZ aluminum nitride (AlN) grown by a high-temperature nitridation method as the model system, dislocation-driven growth was first confirmed by transmission electron microscopy (TEM). Meanwhile numerous stacking faults and associated partial dislocations were also observed and identified to be the Type I stacking faults and the Frank partial dislocations, respectively, using high-resolution TEM. In contrast, AlN NWs obtained by rapid quenching after growth displayed no stacking faults or partial dislocations; instead many of them had voids that were associated with the dislocation-driven growth. On the basis of these observations, we suggest a formation mechanism of stacking faults that originate from dislocation voids during the cooling process in the syntheses. Similar stacking fault features were also observed in other NWs with WZ structure, such as cadmium sulfide (CdS) and zinc oxide (ZnO).

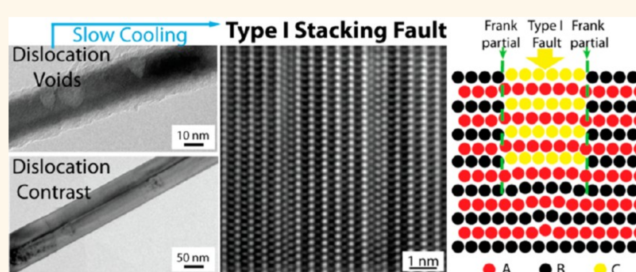

KEYWORDS: stacking fault · partial dislocation · dislocation-driven growth · wurtzite · zinc blende · AlN nanowire

The physical properties and functionality of nanomaterials are dependent on their size, composition, crystal structure, and defect condition. Particularly, polytypic nanowires (NWs), which have uniform chemical composition, but segments of varied crystal structures have tunable electronic band structure and are promising building blocks for nanoscale homojunctions.[1,2] The formation of stacking faults is the key to understanding polytypism in NWs, because stacking faults are present at every boundary between two segments, causing the transition in crystal structures. Indeed, stacking faults have been frequently observed in polytypic NWs of group IV,[3,4] II–VI[5–7] and III–V[8–14] semiconductors, and also in metal NWs.[15] The common feature for most of these materials is that they share the close packed crystal structure, except for the group IV semiconductors which have the diamond structure. For II–VI and III–V compounds, the presence of stacking faults marks the phase transition between hexagonal wurtzite (WZ) and cubic zinc-blende (ZB) structure. The most well-known examples are the "NW twinning superlattices", which are synthesized by catalyst-driven vapor phase growth.[8–11,16,17] In this scenario, catalyst particles drive the anisotropic crystal growth and thus enable the formation of the NW morphology; meanwhile the reaction conditions are carefully tuned to favor the nucleation of either WZ or ZB layers at the interface between the NW and the catalyst.[9]

* Address correspondence to jin@chem.wisc.edu.

Received for review October 7, 2013 and accepted November 26, 2013.

Published online December 02, 2013
10.1021/nn4052293

© 2013 American Chemical Society

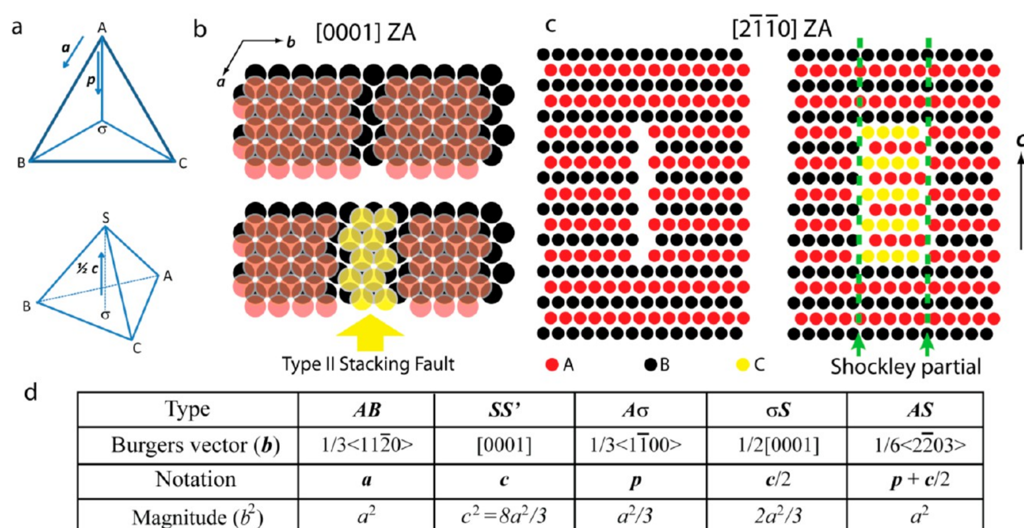

Type	*AB*	*SS'*	*Aσ*	*σS*	*AS*
Burgers vector (***b***)	1/3<11$\bar{2}$0>	[0001]	1/3<1$\bar{1}$00>	1/2[0001]	1/6<$\bar{2}$203>
Notation	***a***	***c***	***p***	***c***/2	***p*** + ***c***/2
Magnitude (b^2)	a^2	$c^2 = 8a^2/3$	$a^2/3$	$2a^2/3$	a^2

Figure 1. Schematic illustrations of (a) common notations used for hcp/WZ lattice, (b and c) dissociation of a perfect dislocation into two Shockley partials in hcp/WZ lattice viewed from [0001] ZA (b) and [2$\bar{1}\bar{1}$0] ZA (c). (d) A table of the common dislocations in hcp/WZ structures.

However, in the absence of catalysts or templates, crystal growth can still occur in a highly anisotropic fashion to form 1D NWs owing to the presence of axial screw dislocations.[18] The screw dislocation-driven growth has been shown to be a general and versatile mechanism to grow NWs and other anisotropic nanostructures of a variety of materials.[19,20] Intriguingly, stacking faults are sometimes also observed in these dislocation-driven NWs.[15,21] It is well-known that dislocations are mobile within a crystal lattice and that the motion and dissociation of a perfect dislocation can lead to the formation of a stacking fault bounded by a pair of Shockley partial dislocations.[22,23] Here we adopt the notation from Berghezan, Fourdeux, and Amelinckx to describe the dislocation vectors in a hexagonal-close-packed (hcp) crystal lattice.[24] As shown in Figure 1a, points A, B, and C represents three adjacent lattice points in a close packed plane, connected by the 1/3 ⟨11$\bar{2}$0⟩ lattice vectors (***a***); σ is the center of the triangle ABC, which is *not* a lattice point, and the vectors **A*σ***, **B*σ***, and **C*σ*** are 1/3 ⟨1$\bar{1}$00⟩ (*p*); S (or S′) is the lattice point in the adjacent close packed plane, whose projection corresponds to the σ point, and the vector ***σ*S** is 1/2[0001] (*c*/2). In theory the possible slip directions in hcp/WZ lattice are linear combinations of the above vectors, which are essentially the Burgers vectors of the dislocations. The table shown in Figure 1d summarizes the most common Burgers vectors in hcp/WZ structures. Note that in the ideal hcp/WZ structures $c = (8/3)^{1/2}a$.

Figure 1b and 1c illustrate the typical dissociation process of a perfect dislocation into two Shockley partial dislocations viewing from the [0001] and [2$\bar{1}\bar{1}$0] zone axes (ZA), respectively. Instead of taking a direct slip motion along the **AB** direction (*a*), the lattice slips along **A*σ*** + ***σ*B** (*p*) because it is energetically more favorable according to Frank's rule: the strain energy associated with a dislocation is proportional to the square of the magnitude of its Burgers vector ($2p^2 = 2a^2/3 < a^2$).[23] The faulted regions (Figure 1b and 1c) generated through this dissociation process are denoted the Type II stacking faults (or intrinsic Type 2, Type I_2 by Lothe and Hirth[22]), which have a characteristic stacking sequence of

...AaBbAaBbAaCcBbCcBbCc...CcBbCcBbCcAaBbAaBb...

where the large and small cases represent the anions and cations in the wurtzite lattice, respectively. Note in these illustrations (Figure 1b and 1c) and discussion we simplify the structural notation to the hcp system, because the motion of the dislocations does not vary a lot between hcp and WZ.

In this article, we report our systematic study of the stacking faults and other crystal defects in wurtzite NWs using AlN NWs as the model system. We choose AlN first because it is a dislocation-prone material and there have been previous reports showing dislocation-driven growth of bulk or micrometer-sized AlN crystals[25,26] and template-free spontaneous formation of AlN nanotubes.[27] Second, AlN is an interesting wide bandgap (6.2 eV) semiconductor that has applications in optoelectronic devices[28,29] and electronic substrates.[30] Finally, AlN is also a robust ceramic material that serves as a mechanical reinforcement phase in metal-matrix nanocomposites.[31,32] The new insights we learned from this study may help to better control the growth of AlN and other WZ nanostructures to enhance their functionality.

RESULTS AND DISCUSSION

Synthesis of AlN NWs. AlN NWs were grown by thermal nitridation of metal aluminum (Al) at 1000 °C and 1 atm

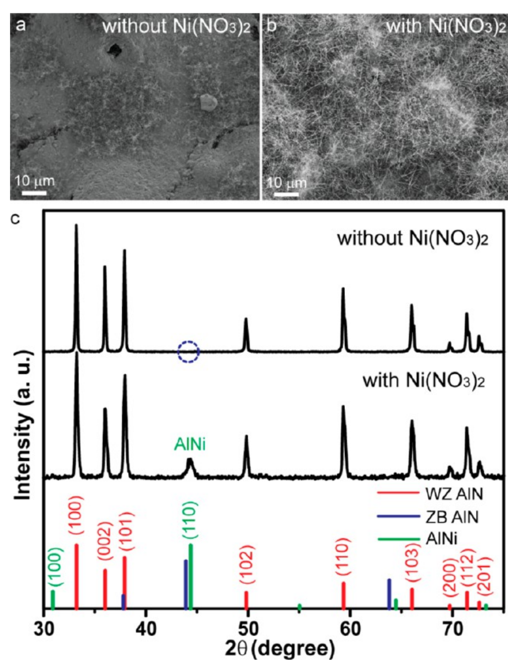

Figure 2. SEM images of the AlN NWs grown without $Ni(NO_3)_2$ (a) and with $Ni(NO_3)_2$ (b). PXRD (c) of AlN NWs and the reference diffractograms.

pressure under the coflow of nitrogen (N_2) and hydrogen (H_2) gas, and then the products were allowed to cool to room temperature naturally under N_2 and H_2 flow. Figure 2a shows a representative scanning electron microscopy (SEM) image of the as-synthesized AlN NWs. Powder X-ray diffraction (PXRD) confirmed that they are phase-pure WZ AlN (PDF No. 25-1133, space group: $P6_3mc$, $a = 0.3111$ nm, $c = 0.4979$ nm, Figure 2c). This also indicates that the as-synthesized NWs are not as heavily faulted as in the cases of the NW twinning superlattices because the ZB AlN peaks (PDF No. 25-1495) were not observed.

The addition of ammonium chloride (NH_4Cl) to the Al powder was crucial for the growth of AlN NWs, which facilitated the transportation of Al into the vapor phase and the further reaction with N_2. When no NH_4Cl was added or other ammonium/amine containing compounds such as NH_4HCO_3 or urea were used as ammonia source instead of the chloride salt, growth of NWs was not observed. The possible chemical reactions involved in this synthesis are listed as follows:

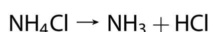

$$NH_4Cl \rightarrow NH_3 + HCl$$

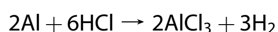

$$2Al + 6HCl \rightarrow 2AlCl_3 + 3H_2$$

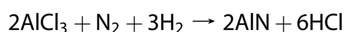

$$2AlCl_3 + N_2 + 3H_2 \rightarrow 2AlN + 6HCl$$

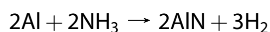

$$2Al + 2NH_3 \rightarrow 2AlN + 3H_2$$

The sublimation and decomposition of NH_4Cl starts at around 350 °C, resulting in a white cloud that moves downstream inside the tube. The generation of HCl vapor leads to the formation of $AlCl_3$, which acts as a vapor transfer reagent that further reacts with gaseous N_2 to yield AlN. Indeed, N_2 flow is necessary, since pure Al is obtained using Ar as carrier gas (data not shown), confirming that the nitrogen in AlN mainly comes from N_2 flow rather than NH_4Cl. The coflow of H_2 gas has dual roles here: first the H_2 is involved in the reactions that form AlN, which affects the chemical equilibrium and supersaturation of the reaction system; second it has been pointed out that the introduction of H_2 gas in the vapor-phase syntheses of NWs often facilitates the dislocation-driven growth mechanism.[18,19,21,33,34]

TABLE 1. Statistics on Growth Directions of AlN NWs

	$\langle 0001 \rangle$	$\langle 10\bar{1}0 \rangle$	$\langle 10\bar{1}1 \rangle$	total
without $Ni(NO_3)_2$	89	63	77	229
with $Ni(NO_3)_2$	68	64	8	140

The introduction of a small amount of nickel(II) nitrate [$Ni(NO_3)_2$] increases the yield of AlN NWs (Figure 2b), nevertheless it was not a necessary condition for the NW growth. We would like to point out that the Ni herein was likely not a catalyst in the typical vapor−liquid−solid growth, because catalyst tips were not observed. We also did not detect signals of Ni in these NWs by either energy-dispersive spectroscopy (EDS, Supporting Information, Figures S1 and S2) or electron energy loss spectroscopy (EELS, Figure S3) using TEM and scanning transmission electron microscopy (STEM). In the PXRD there was emergence of peaks attributed to the AlNi alloy (PDF No. 20-0019, space group: $Pm\bar{3}m$, $a = 0.2887$ nm, Figure 2c), which was probably present in the form of other morphologies. It is possible that the mixing of Ni impurities lowers the nucleation energy and thus promotes the subsequent growth of AlN NWs, as we have observed before for the growth of CdS and CdSe NWs with the presence of Au.[21]

Using transmission electron microscopy (TEM), we observed three major growth directions for these AlN NWs: $\langle 0001 \rangle$, $\langle 10\bar{1}0 \rangle$, and $\langle 10\bar{1}1 \rangle$, all of which are common directions of dislocation Burgers vectors in WZ lattice (Table 1). The addition of $Ni(NO_3)_2$ clearly suppressed the growth of AlN NWs along the $\langle 10\bar{1}1 \rangle$ direction, and $\langle 0001 \rangle$ and $\langle 10\bar{1}0 \rangle$ dominate the growth directions (the statistics are shown in Table 1), which is likely due to the change in the initial nucleation caused by the introduction of Ni impurities, for example, the formation of AlNi phase in the "seeding layer". Otherwise, the difference in the NWs grown with or without $Ni(NO_3)_2$ is not significant: dislocations and stacking faults are present in both cases. Therefore we do not specifically distinguish growth conditions for the NWs shown in the rest of the discussion.

Confirmation of the Dislocation-Driven Growth of AlN NWs. Diffraction contrast transmission electron microscopy (DCTEM) was employed to confirm the

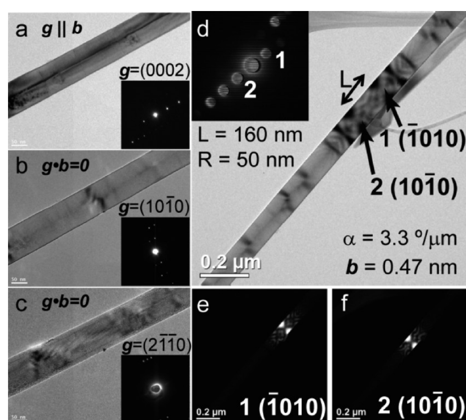

Figure 3. Structural confirmation of screw dislocation-driven growth of AlN NWs and the Eshelby twist: (a–c) Diffraction contrast TEM imaging of the dislocation in an AlN NW under strong two-beam conditions. Panel a represents the $g||b$ condition when the dislocation contrast is the strongest; panels b and c represent invisibility conditions when the dislocation contrast disappears. (d–f) Eshelby twist contour analysis of another AlN NW. Panel d shows the bright-field image of a NW with multiple dark bands of twist contours and the relevant measurements of them; panels e and f show the dark-field index of a pair of the contour bands. Insets are the corresponding selected area electron diffraction (SAED) patterns.

dislocation-driven growth of as-synthesized AlN NWs. The presence of an axial screw dislocation distorts the lattice planes at the core of the NW, which deflects away incident electrons, generating a dark line of contrast. However, this dislocation contrast is not visible when only reciprocal space lattice vectors (g vectors) that are orthogonal to the Burgers vector (b) are excited ($g \cdot b = 0$, the invisibility criterion).[35] Therefore the direction of a dislocation can be determined by taking the cross product of two noncollinear g vectors that meet the invisibility criterion ($b||g_1 \times g_2$). The AlN NW displayed no dislocation contrast when two beam conditions of $g = (10\bar{1}0)$ (Figure 3b) and $g = (2\bar{1}\bar{1}0)$ (Figure 3c) were established, and the characteristic dislocation contrast line was clearly observed when $g = (0002)$ was excited (Figure 3a). The Burgers vector can then be identified to be along [0001] directions. In addition to the pure axial screw dislocations observed in NWs growing along the [0001] directions, dislocations with a mixture of edge and screw components were also seen in the NWs growing along the $[10\bar{1}0]$ directions (see Supporting Information, Figure S4), accounting for the anisotropic growth of the nanostructure.

The Eshelby twist is another signature of the dislocation-driven growth, which is caused by the strain field in the crystal lattice introduced by the presence of screw dislocations.[36] We also detected and quantified the Eshelby twist in these AlN NWs using twist contour analysis,[26] the principle and procedure of which have been discussed in detail in our previous work.[37,38] For the AlN NW shown in Figure 3d, it is twisted 3.3° per micrometer, which corresponds to a Burgers vector of 0.47 nm in magnitude which is approximately the length of (0001) spacing in AlN (c = 0.4979 nm). These confirm the operation of the screw dislocation-driven mechanism in the growth of AlN NWs.

Observation of Stacking Faults in AlN NWs. We would like to point out that only a small portion of the examined NWs (12 out of 369) display distinctive dislocation contrast. However, in the rest of the AlN NWs that do not display axial screw dislocations, stacking faults are frequently observed (97 out of 369, ~26%). The stacking faults always dwell on the {0001} planes (the close packed plane), regardless of the growth directions of AlN NWs, which is commonly observed in ionic wurtzite crystals. The $\{11\bar{2}0\}$ prismatic faults were rarely reported for AlN, except for an early report by Drum on intersecting faults in AlN film.[39] Figure 4a to 4d show typical features of stacking faults (marked by orange arrows) observed under TEM in NWs growing along [0001] (Figure 4a and 4b), $[10\bar{1}0]$ (Figure 4c), and $[10\bar{1}1]$ (Figure 4d) directions, respectively. More intriguingly, many stacking faults are bound by partial dislocations (Figure 4e to 4h), which are generally recognized as the extended dislocations. Among these stacking faults or extended dislocations, it is most common that they form a closed loop with the direction of partial dislocations perpendicular to the faulted planes, rendering as a concave feature on the surface of the NW (Figure 4e and 4f). Occasionally there are zigzag features, where stacking faults are connected by partial dislocations (Figure 4g and 4h). Note that stacking faults that occupy a partial crystal plane can appear to be completely filling a layer when viewed from certain direction (Supporting Information, Figure S5). The mutually exclusive appearance of the threading screw dislocations and stacking faults with partial dislocations in these AlN NWs make us wonder if there is a causal relation between these two phenomena: could the original screw dislocation move and/or dissociate and lead to the formation of extended dislocations?

Identification of the Stacking Faults and Discussion of Their Formation Mechanisms. Steinberger et al. suggested a mechanism for giant screw dislocations in zinc-blende ZnS crystals that have Burgers vectors of $2nc$ ($n \geq 1$) to dissociate into Shockley partials *via* a periodic slip process during the cooling down of crystal growth, resulting in polytypic crystals.[40,41] If this hypothesis also held true in our case of AlN NWs, we would expect the partial dislocations to be the Shockley type and the enclosed stacking fault region to be Type II, as shown in the schemes in Figure 1. Therefore we set out to use high-resolution TEM (HRTEM) to carefully examine the classification of the stacking faults in the AlN NWs to verify the hypothesis above. The NWs were first tilted onto the $[2\bar{1}\bar{1}0]$ zone axis of AlN, which is the proper orientation to observe and distinguish the stacking sequences. To increase the signal-to-noise of the lattice

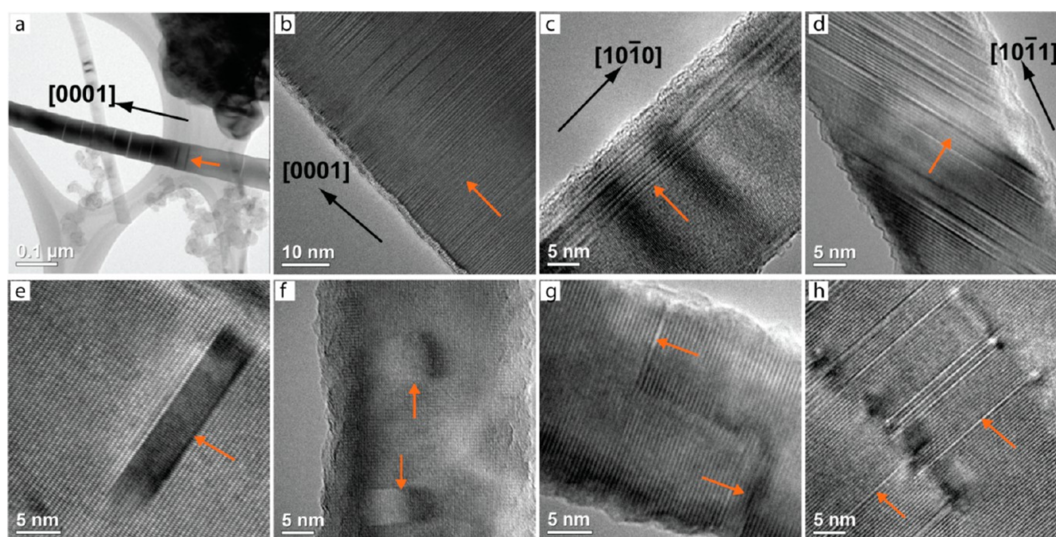

Figure 4. A collection of TEM images showing representative stacking fault features in the AlN NWs: (a–d) Generic stacking fault features in NWs growing along [0001] (a and b), [10$\bar{1}$0] (c), and [10$\bar{1}$0] (d) directions. (e–h) Stacking faults bounded by partials dislocations. The stacking fault regions are marked by the orange arrows. Note that NWs shown in panels g and h are from a slightly different synthesis (see Methods section).

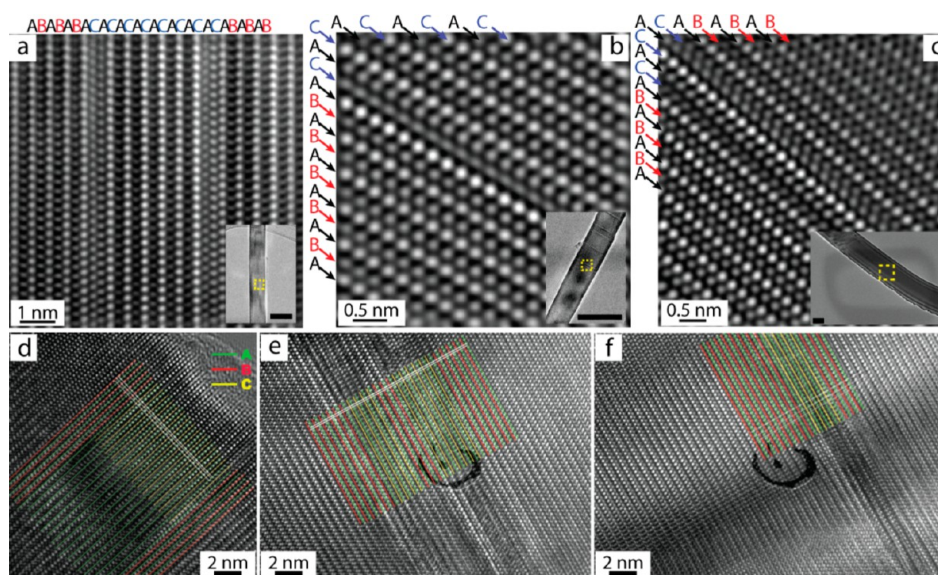

Figure 5. Identification of Type I stacking faults in the AlN NWs. The yellow dashed squared in the insets represent the region from which the HRTEM were acquired. All of the scale bars in the insets are 50 nm. Note that the circular features in panels e and f are due to a defect in the CCD camera of the TEM.

fringes, Fourier filtering was applied to all of the HRTEM images shown in Figure 4, which specifically selected $\{0002\}$ and $\{10\bar{1}0\}$ reciprocal space lattice vectors. However, the identification of various stacking faults in the AlN NWs reveals *all* of them to be Type I, with a stacking sequence of

...AaBbAaBbAaCcAaCcAa...AaCcAaCcAaBbAaBb...

Unlike the Type II stacking faults, the Type I has one set of close packing layer that stays in its correct position (the A layer, *e.g.*) and the other two alternating their positions (B and C layer) across the boundary between faulted and unfaulted regions. Here we show the most generic Type I arrangement in AlN NWs growing along [10$\bar{1}$0] crystal axes (Figure 5a,c) or [0001] (Figure 5b), which clearly possesses the above characteristics. The stacking faults in these two images did not terminate within the NWs, therefore no bounding partial dislocations were observed. The stacking faults with closed loop shape (Figure 5d–f) are indexed to be the Type I as well, enclosed by the Frank-type of partial dislocations that possess a screw component ($p + c/2$). These HRTEM features of Type I stacking fault and Frank partial dislocations are also consistent with the previous report on TEM imaging of stacking faults in wurtzite crystals.[42] The unequivocal identification of

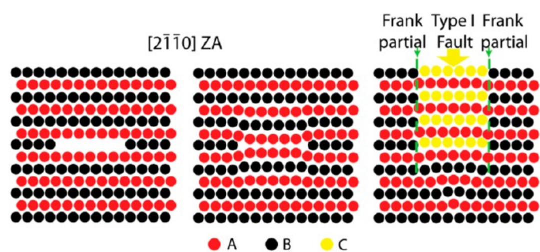

Figure 6. Schematic illustration of the formation of a Type I stacking fault and its associated Frank partial dislocation pairs by collapsing on a void in the hcp/WZ crystal lattice.

the Type I stacking fault and the Frank partial dislocations disapprove our initial speculation that the stacking faults directly evolve from the dissociation of dislocations.

The natural question to ask next is, Could these stacking faults simply be "growth defects"? Here the "growth defects" specifically refer to the defects that are generated during the crystal growth due to fluctuation of the supersaturation, as opposed to defects that are introduced by postgrowth treatment such as quenching or mechanical compression. These growth defects do not necessarily play a role in the anisotropic growth. Calculation shows that in general the formation energy of Type I stacking fault is smaller than that of Type II,[43] because it only requires one operation of faulted nucleation to form Type I stacking fault, whereas the formation of Type II stacking fault relies on two successive faulted nucleations. Therefore ideally the formation of Type I stacking fault by crystal growth is thermodynamically favored over the Type II. However, in reality the coexistence of both Type I and Type II stacking faults has always been observed in as-grown crystals, in either thin film or nanostructures.[44−48] Also Amelinckx *et al*. pointed out the possibility of forming a Type II stacking fault in the growth conditions close to the transition point between WZ and ZB phases.[44] Most importantly, in all of the above discussion of the "growth defects", the supersaturation levels of the growth ambient are sufficiently high and it is essentially the layer-by-layer mechanism that dominates crystal growths as well as the formation of stacking faults, whereas in our growth of AlN NWs, we have confirmed that the dislocation-driven mechanism is playing a significant role, indicating a relatively low supersaturation. By all accounts, the appearance of *exclusively* Type I stacking faults in the AlN NWs *cannot* be simply attributed to the "growth defects".

An alternative route to form a Type I stacking fault is by collapsing atomic layers around vacancies or voids in the crystal lattice as illustrated in Figure 6. In the case of a voided disk of one atomic layer thick, both "A" planes below and above the vacancy will become close simultaneously at the beginning (middle panel of Figure 6), and one of them will collapse to become a "C" stacking layer eventually. This process typically occurs during the course of cooling crystals from higher growth temperature,[23] which is an aspect in the crystal growth that people usually overlook. On the other hand, the dislocation-driven growth can lead to the formation of hollow structures or voids when the Burgers vectors are large, also known as the "open-core dislocations".[49,50] In 1D nanostructures, the appearance of hollow nanotubes or voided nanowires is associated with the dislocation-driven growth mechanism.[15,19,38,51−54] We then realized that in the typical syntheses of these AlN NWs with Type I stacking faults, the products were allowed to cool down from 1000 °C to room temperature naturally, which took about 30 to 40 min. Therefore, we speculate that the formation of Type I stacking faults and the associated Frank partial dislocations might take place during this cooling process, if the as-grown AlN NWs had indeed been voided.

Quenching the AlN NWs. To test our new hypothesis that the formation of stacking faults from voids occur during the cooling process, we tried to rapidly quench the growth products from high temperature to room temperature by taking out the reaction boat while it was still at 1000 °C and then quickly putting it onto a pile of dry ice. In this way the product could be cooled down to the room temperature in less than 30 s, which essentially shut down the pathway to form Type I stacking faults during the slow cooling process and "froze" the NWs in their as-grown forms. TEM examination showed that the quenched AlN NWs exhibited rather different characteristics than the ones collected after slow cooling (Figure 7).

The major observations are summarized as follows:

(1) The quenched NWs are still single crystals of WZ AlN. This was confirmed by HRTEM, as shown in the Supporting Information (Figure S6). The major growth directions of the quenched AlN NWs are along [0001] and [10$\bar{1}$0], which is consistent with the distribution of the unquenched NWs. There was clearly oxide layer formation on the NWs due to exposure to air when the product was still red-hot. This was not seen in the naturally cooled samples, because the coflow of nitrogen and hydrogen was kept on, which protected the NWs from being oxidized.

(2) Many quenched NWs (10 out of 53 NWs examined, ~19%) have nanometer-sized voids in the middle (Figure 7a−e), which is not observed for the NWs cooled down slowly. This percentage is comparable but slightly lower than the ratio of NWs with stacking faults in the naturally cooled samples (~26%). This is consistent with our hypothesis. These voids are likely the consequence and signature of the dislocation-driven growth mechanism, and later on become the sites where the lattice collapsing happens, and evolve into the Type I stacking faults and associated Frank partial dislocations if the NWs were allowed to cool down naturally.

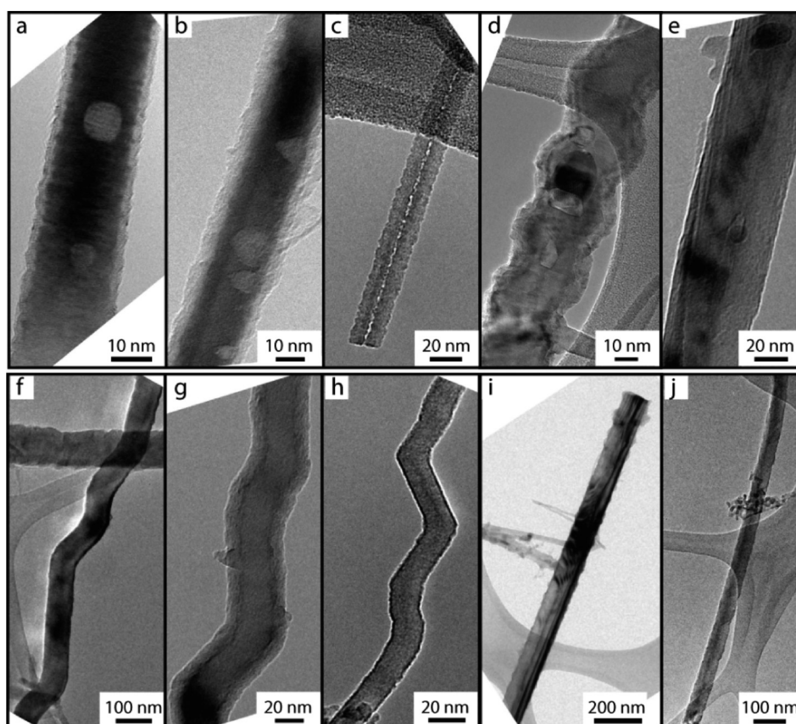

Figure 7. Representative TEM images of the AlN NWs obtained by quenching the growth at high temperature: (a−e) NWs with nanometer-sized holes; (f−h) helical NWs; (i,j) NWs displaying dislocation contrast.

(3) There is no noticeable feature of stacking faults observed in the quenched NWs, which is another significant difference from those NWs that underwent natural cooling. This is confirmed by SAED and HRTEM observation near the $[2\bar{1}\bar{1}0]$ zone axis (Supporting Information, Figure S6). If there were stacking faults in the NW, the $\{0001\}$ diffraction spots would have extended to a string of spots, which did not occur in the quenched NWs. This further confirms that the growth conditions employed herein still lie in the relatively low supersaturation regime, and that the Type I stacking faults observed are indeed not induced by growth.

(4) Some helical structures (5 out of 53) were observed (Figure 7f−h), which was not seen previously. SAED confirmed that they were indeed helices (Supporting Information, Figure S7), as there was a rotational change in the brightness of the diffraction spots. The emergence of this new morphology is beyond our understanding. Although it is visually intuitive to correlate the helical feature with screw dislocations and therefore the dislocation-driven mechanism, we do not have enough information to explain how the helices relax to become straight wires during a slow cooling process, and might have connection with the stacking faults. Furthermore, similar helical (or zigzag) features in AlN NWs have also been reported by other groups where natural cooling was adopted.[55,56] Hence it is unlikely that the quenching process leads to the formation of these structures.

(5) Axial screw dislocation contrast could still be observed (2 out of 53) in the quenched NWs (Figure 7i,j). This confirms that the quenching treatment does not affect the way NWs grows, and that it is unlikely the axial screw dislocations are introduced in the cooling process.

The emergence of voids and absence of stacking faults in the quenched AlN NWs are consistent with our hypothesis that the Type I stacking faults and partial dislocations form during the process of the postgrowth cooling process rather than the crystal growth. However, at present we cannot completely eliminate side effects caused by the quenching treatment, for example, the generation of oxide layers and possible chemical stress induced by the temperature gradient, *etc.* The ideal way to unequivocally prove the hypothesis is by *in situ* environmental TEM and HRTEM observation of the whole course of the growth and cooling processes,[57] which is beyond our capability. Nevertheless, the evidence we have presented are all consistent and strongly suggest the possibility of forming stacking fault defects in crystals/NWs from voids during postgrowth processes that people usually overlook.

Observation of Type I Stacking Faults in Other Wurtzite NWs. We would like to point out that even though our experimental work was focused on AlN NWs, this mechanism of forming stacking faults in dislocation-driven materials is general to other dislocation-prone WZ NWs, such as other II−VI[21,51] and III−V compounds.[58−60] As a preliminary study, we have also looked into the stacking fault structures of other NWs of WZ structures including cadmium sulfide (CdS) and

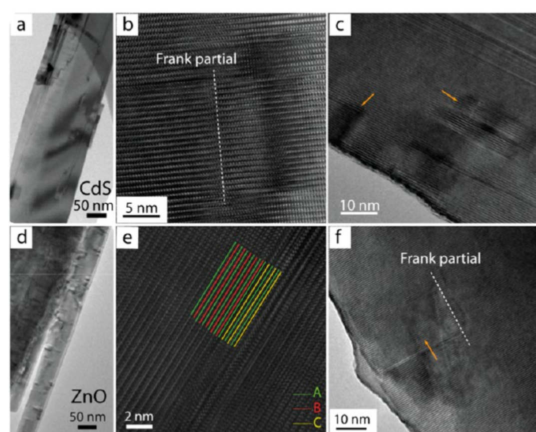

Figure 8. Type I stacking faults and Frank partial dislocations in CdS (a−c) and ZnO (d−f) NWs. (a) Low-resolution TEM image of a CdS NW containing zigzag-shaped stacking faults. (b) HRTEM image showing the faulted region in panel a with a Frank partial dislocation. (c) HRTEM image of a CdS NW containing closed-loop stacking faults. (d) Low-resolution TEM image of a ZnO NW containing closed-loop stacking faults. (e) HRTEM image showing the index of Type I stacking fault in the ZnO NW shown in panel d. (f) HRTEM image showing the Frank partial dislocation in a ZnO NW. Orange arrows indicate the faulted region.

zinc oxide (ZnO), and found them to be the Type I as well. The CdS NWs (Figure 8a−c) were synthesized by thermal evaporation of CdS powder. The ZnO NWs (Figure 8d−f) were epitaxially grown in aqueous solution from microplates of copper gallium oxide ($CuGaO_2$).[61] The low-resolution TEM images of CdS and ZnO NWs (Figure 8a,d) show typical Type I stacking faults with Frank partial dislocations that have zigzag shape (Figure 8a) or closed loop shape (Figure 8d), which are visually similar to what have been observed in the AlN NWs. HRTEM (Figure 8b,c,e,f) further confirms the identification of the Type I arrangement as well as the Frank-type partial dislocations in these NWs. Meanwhile, several other reported WZ NWs[62,63] grown by catalyst-free methods also exhibited the stacking fault features that might be indexed to the Type I. Interestingly, most of these catalyst-free NW growths that led to the formation of stacking faults (Type I) were high temperature vapor phase growth, suggesting the disparity in growth temperatures might be the cause of the difference. However, the ZnO we examined were grown from a low temperature aqueous solution. We need to consider two factors: (i) the growth conditions for ZnO have been shown to produce hollow structures, contributing to additional surface energy;[51] (ii) ZnO has a relatively small stacking fault energy compared with AlN.[42] The formation of Type I stacking faults might compensate for the surface energy and enable the process at low temperature. Depending on the relative energetics of stacking faults and dislocations, the frequency of stacking fault observation might vary between different materials.

CONCLUSION AND OUTLOOK

We have carefully and systematically examined the stacking fault and dislocation defects in AlN NWs that have been synthesized *via* a high-temperature, catalyst-free, vapor phase growth. We confirmed the operation of the dislocation-driven growth in these AlN NWs by diffraction-contrast TEM as well as Eshelby twist contour analysis. More importantly, we also observed and investigated stacking faults and the associated partial dislocations in the as-grown NWs. All of the stacking faults were identified to be Type I, and the associated partial dislocations were identified as Frank-type using HRTEM characterization. These defects cannot be explained by the classic route of dissociating a perfect dislocation. However, Type I stacking faults can form by collapsing around voids in the crystal lattice during a slow cooling process. The AlN NWs that are grown driven by dislocations could generate voids that further evolve into Type I stacking faults and the associated Frank partial dislocations. We indeed observed voids in the AlN NWs by rapidly cooling the NW products from high temperature to avoid the evolution of extended defects and to preserve the original structural characteristics present during crystal growth, which strongly suggests that the stacking faults observed are formed during the postgrowth cooling process. This new understanding of stacking fault formation can also be applied to NWs of other wurtzite materials, such as CdS and ZnO, in which similar Type I stacking faults and Frank partial dislocations have been preliminarily observed. More advanced microscopy technique, such as *in situ* environmental TEM, might provide a more direct and definitive proof of the proposed hypothesis. Understanding the origins and formation mechanisms of stacking fault defects will enable us to rationally control them in AlN, CdS, ZnO, and other WZ nanostructures and therefore allow us to better realize desired physical properties for specific applications.

METHODS

Materials. All chemicals were purchased from Sigma-Aldrich and used as received without further purification.

Synthesis of AlN NWs. Most of the AlN NW samples we examined were synthesized *via* the thermal nitridation of metal Al powder. In a typical synthesis, 0.500 g of metal Al powder, 0.500 g of NH_4Cl, and 0.100 g of $Ni(NO_3)_2 \cdot 6H_2O$ (if used) were mixed and ground in a mortar and then transferred into an alumina boat. The boat was placed in a quartz tube (1 in. i.d.) connected to N_2 and H_2 gas inlets and the exhaust line in a vacuum system. The tube was placed in a tube furnace (Thermal Fisher, Lindberg Blue), and the reaction boat was at the center of

ARTICLE

the furnace. The system was flushed with a coflow of 480 sccm N_2 and 20 sccm H_2 for 30 min prior to heating. Then the temperature was raised to 1000 °C from room temperature at a rate of 15 °C/min and held at 1000 °C for 1 h. After the reaction was finished, the furnace was opened to allow the reaction tube to naturally cool to room temperature under N_2 and H_2 flow. In the case of a quenched reaction, the reaction boat was taken out of the tube immediately while it was still at 1000 °C and then put onto a pile of dry ice. Some AlN NW samples examined (Figure 3 panels g and h) were synthesized following a modified synthesis that was described in a previous work.[27] Briefly, Al powder was dipped into a solution of $CoSO_4$. After the solvent was evaporated, $CoSO_4$-impregnated Al powder was obtained (0.8 mmol Co/g Al). Then, the precursor was put into a tube furnace, which was heated up to 1150 °C under the protection of 100 sccm Ar. When the temperature reached 970 °C, 200 sccm NH_3/N_2 (NH_3 4 vol %) gas was introduced into the system as the nitrogen source. The reaction lasted for 90 min, and then the furnace was cooled naturally.

Synthesis of CdS NWs. The CdS NWs were synthesized by coevaporation of CdS powder and metal Bi powder at 650 °C under the coflow of 100 sccm Ar gas and 20 sccm H_2 gas at 1 Torr. We note that in this synthesis there is coexistence of the dislocation-driven growth and the VLS growth. Nevertheless, we intentionally examined the defects using TEM on the NWs that were free of the catalyst tips, whose growth were more likely to be driven by the screw dislocations.

Synthesis of ZnO NWs. The ZnO NWs were synthesized by hydrolysis of $Zn(NO_3)_2$ under the presence of hexamethylenetetramine (HMT) in an aqueous solution, as described previously.[61]

Structural Characterization. SEM was performed using a LEO Supra55 VP microscope. PXRD data were collected on AlN NWs dispersed on glass substrates using a Siemens STOE diffractometer with Cu Kα radiation. TEM samples were prepared by gently vortexing and dropcasting the NW samples onto lacey carbon-supported TEM grids. An FEI Titan scanning transmission electron microscope (200 kV), an FEI TF-30 transmission electron microscope (300 kV), and a Philips CM-200 transmission electron microscope (200 kV) were used for the microstructural analysis of the AlN, CdS, and ZnO NWs.

Conflict of Interest: The authors declare no competing financial interest.

Acknowledgment. This research is supported by NSF DMR-1106184 (F.M. and S.J.). M.E. contributed to the AlN NW synthesis and was supported by the US Department of Commerce National Institute of Standards and Technology (NIST) through its Technology Innovation Program (Grant No. 70NANB10H003). A.F. synthesized the ZnO NWs and was supported by the University of Wisconsin—Madison NSEC (NSF DMR 0832760). Q.W. and Z.H. synthesized some of the AlN samples and thank NSFC (21073085) and "973" programs (2013CB932902) for support. S.J. also thanks the Research Corporation ScialLog Award for Solar Energy Conversion and UW-Madison Vilas Associate Award for support.

Supporting Information Available: STEM-EDS mapping and EELS of AlN NWs, diffraction-contrast TEM images of an AlN NW growing along the [$10\bar{1}0$] direction, a schematic illustration of partial stacking faults, and additional HRTEM images and ED patterns of quenched AlN NWs and helices. This material is available free of charge *via* the Internet at http://pubs.acs.org.

REFERENCES AND NOTES

1. Murayama, M.; Nakayama, T. Electronic-Structures of Hetero-Crystalline Semiconductor Superlattices. *J. Phys. Soc. Jpn.* **1992**, *61*, 2419–2433.
2. Murayama, M.; Nakayama, T. Chemical Trend of Band Offsets at Wurtzite Zincblende Heterocrystalline Semiconductor Interfaces. *Phys. Rev. B* **1994**, *49*, 4710–4724.
3. Lopez, F. J.; Givan, U.; Connell, J. G.; Lauhon, L. J. Silicon Nanowire Polytypes: Identification by Raman Spectroscopy, Generation Mechanism, and Misfit Strain in Homostructures. *ACS Nano* **2011**, *5*, 8958–8966.
4. Jeon, N.; Dayeh, S. A.; Lauhon, L. J. Origin of Polytype Formation in VLS-Grown Ge Nanowires through Defect Generation and Nanowire Kinking. *Nano Lett.* **2013**, *13*, 3947–3952.
5. Utama, M. I. B.; Peng, Z. P.; Chen, R.; Peng, B.; Xu, X. L.; Dong, Y. J.; Wong, L. M.; Wang, S. J.; Sun, H. D.; Xiong, Q. H. Vertically Aligned Cadmium Chalcogenide Nanowire Arrays on Muscovite Mica: A Demonstration of Epitaxial Growth Strategy. *Nano Lett.* **2011**, *11*, 3051–3057.
6. Utama, M. I. B.; Zhang, Q.; Jia, S. F.; Li, D. H.; Wang, J. B.; Xiong, Q. H. Epitaxial II−VI Tripod Nanocrystals: A Generalization of van der Waals Epitaxy for Nonplanar Polytypic Nanoarchitectures. *ACS Nano* **2012**, *6*, 2281–2288.
7. Utama, M. I. B.; de la Mata, M.; Magen, C.; Arbiol, J.; Xiong, Q. H. Twinning-, Polytypism-, and Polarity-Induced Morphological Modulation in Nonplanar Nanostructures with van der Waals Epitaxy. *Adv. Funct. Mater.* **2013**, *23*, 1636–1646.
8. Johansson, J.; Karlsson, L. S.; Svensson, C. P. T.; Martensson, T.; Wacaser, B. A.; Deppert, K.; Samuelson, L.; Seifert, W. Structural Properties of (111)B-oriented III−V Nanowires. *Nat. Mater.* **2006**, *5*, 574–580.
9. Caroff, P.; Dick, K. A.; Johansson, J.; Messing, M. E.; Deppert, K.; Samuelson, L. Controlled Polytypic and Twin-Plane Superlattices in III−V Nanowires. *Nat. Nanotechnol.* **2009**, *4*, 50–55.
10. Algra, R. E.; Verheijen, M. A.; Borgstrom, M. T.; Feiner, L. F.; Immink, G.; van Enckevort, W. J. P.; Vlieg, E.; Bakkers, E. P. A. M. Twinning Superlattices in Indium Phosphide Nanowires. *Nature* **2008**, *456*, 369–372.
11. Dick, K. A.; Thelander, C.; Samuelson, L.; Caroff, P. Crystal Phase Engineering in Single InAs Nanowires. *Nano Lett.* **2010**, *10*, 3494–3499.
12. Kitauchi, Y.; Kobayashi, Y.; Tomioka, K.; Hara, S.; Hiruma, K.; Fukui, T.; Motohisa, J. Structural Transition in Indium Phosphide Nanowires. *Nano Lett.* **2010**, *10*, 1699–1703.
13. Ikejiri, K.; Kitauchi, Y.; Tomioka, K.; Motohisa, J.; Fukui, T. Zinc Blende and Wurtzite Crystal Phase Mixing and Transition in Indium Phosphide Nanowires. *Nano Lett.* **2011**, *11*, 4314–4318.
14. Spirkoska, D.; Arbiol, J.; Gustafsson, A.; Conesa-Boj, S.; Glas, F.; Zardo, I.; Heigoldt, M.; Gass, M. H.; Bleloch, A. L.; Estrade, S.; *et al.* Structural and Optical Properties of High Quality Zinc-Blende/Wurtzite GaAs Nanowire Heterostructures. *Phys. Rev. B* **2009**, *80*, 245325.
15. Meng, F.; Jin, S. The Solution Growth of Copper Nanowires and Nanotubes Is Driven by Screw Dislocations. *Nano Lett.* **2012**, *12*, 234–239.
16. Burgess, T.; Breuer, S.; Caroff, P.; Wong, J.; Gao, Q.; Tan, H. H.; Jagadish, C. Twinning Superlattice Formation in GaAs Nanowires. *ACS Nano* **2013**, *7*, 8105–8114.
17. Xiong, Q. H.; Wang, J.; Eklund, P. C. Coherent Twinning Phenomena: Towards Twinning Superlattices in III−V Semiconducting Nanowires. *Nano Lett.* **2006**, *6*, 2736–2742.
18. Bierman, M. J.; Lau, Y. K. A.; Kvit, A. V.; Schmitt, A. L.; Jin, S. Dislocation-Driven Nanowire Growth and Eshelby Twist. *Science* **2008**, *320*, 1060–1063.
19. Meng, F.; Morin, S. A.; Forticaux, A.; Jin, S. Screw Dislocation Driven Growth of Nanomaterials. *Acc. Chem. Res.* **2013**, *46*, 1616–1626.
20. Jin, S.; Bierman, M. J.; Morin, S. A. A New Twist on Nanowire Formation: Screw-Dislocation-Driven Growth of Nanowires and Nanotubes. *J. Phys. Chem. Lett.* **2010**, *1*, 1472–1480.
21. Wu, H.; Meng, F.; Li, L.; Jin, S.; Zheng, G. Dislocation-Driven CdS and CdSe Nanowire Growth. *ACS Nano* **2012**, *6*, 4461–4468.
22. Hirth, J. R.; Lothe, J. *Theory of Dislocations*; McGraw-Hill: New York, 1968.
23. Hull, D.; Bacon, D. J. *Introduction to Dislocations*; 5th ed.; Elsevier: Oxford, 2011.
24. Berghezan, A.; Fourdeux, A.; Amelinckx, S. Transmission Electron Microscopy Studies of Dislocations and Stacking Faults in a Hexagonal Metal: Zinc. *Acta Metal.* **1961**, *9*, 464–490.

25. Drum, C. M. Axial Imperfections in Filamentary Crystals of Aluminum Nitride .I. *J. Appl. Phys.* **1965**, *36*, 816–823.
26. Drum, C. M. Twist and Axial Imperfections in Filamentary Crystals of Aluminum Nitride. II. *J. Appl. Phys.* **1965**, *36*, 824–829.
27. Wu, Q.; Hu, Z.; Wang, X.; Lu, Y.; Chen, X.; Xu, H.; Chen, Y. Synthesis and Characterization of Faceted Hexagonal Aluminum Nitride Nanotubes. *J. Am. Chem. Soc.* **2003**, *125*, 10176–10177.
28. Taniyasu, Y.; Kasu, M.; Makimoto, T. An Aluminium Nitride Light-Emitting Diode with a Wavelength of 210 Nanometres. *Nature* **2006**, *441*, 325–328.
29. Ponce, F. A.; Bour, D. P. Nitride-Based Semiconductors for Blue and Green Light-Emitting Devices. *Nature* **1997**, *386*, 351–359.
30. Bondokov, R. T.; Mueller, S. G.; Morgan, K. E.; Slack, G. A.; Schujman, S.; Wood, M. C.; Smart, J. A.; Schowalter, L. J. Large-Area AlN Substrates for Electronic Applications: An Industrial Perspective. *J. Cryst. Growth* **2008**, *310*, 4020–4026.
31. Cao, G.; Choi, H.; Oportus, J.; Konishi, H.; Li, X. Study on Tensile Properties and Microstructure of Cast AZ91D/AlN Nanocomposites. *Mater. Sci. Eng. A—Struct.* **2008**, *494*, 127–131.
32. Liu, Y. Q.; Cong, H. T.; Wang, W.; Sun, C. H.; Cheng, H. M. AlN Nanoparticle-Reinforced Nanocrystalline Al Matrix Composites: Fabrication and Mechanical Properties. *Mater. Sci. Eng. A* **2009**, *505*, 151–156.
33. Zhu, J.; Peng, H.; Marshall, A. F.; Barnett, D. M.; Nix, W. D.; Cui, Y. Formation of Chiral Branched Nanowires by the Eshelby Twist. *Nat. Nanotechnol.* **2008**, *3*, 477–481.
34. Lau, Y. K. A.; Chernak, D. J.; Bierman, M. J.; Jin, S. Formation of PbS Nanowire Pine Trees Driven by Screw Dislocations. *J. Am. Chem. Soc.* **2009**, *131*, 16461–16471.
35. Williams, D. B.; Carter, C. B. *Transmission Electron Microscopy: A Textbook for Materials Science*; 1st ed.; Plenum Press: New York, 1996.
36. Eshelby, J. D. The Twist in a Crystal Whisker Containing a Dislocation. *Philos. Mag.* **1958**, *3*, 440–447.
37. Morin, S. A.; Jin, S. Screw Dislocation-Driven Epitaxial Solution Growth of ZnO Nanowires Seeded by Dislocations in GaN Substrates. *Nano Lett.* **2010**, *10*, 3459–3463.
38. Meng, F.; Morin, S. A.; Jin, S. Rational Solution Growth of α-FeOOH Nanowires Driven by Screw Dislocations and Their Conversion to α-Fe_2O_3 Nanowires. *J. Am. Chem. Soc.* **2011**, *133*, 8408–8411.
39. Drum, C. M. Intersecting Faults on Basal and Prismatic Planes in Aluminium Nitride. *Philos. Mag.* **1965**, *11*, 313–&.
40. Mardix, S.; Kalman, Z. H.; Steinberger, I. T. Periodic Slip Processes and the Formation of Polytypes in Zinc Sulphide Crystals. *Acta Crystallogr.* **1968**, *24*, 464–469.
41. Alexander, E.; Kalman, Z. H.; Mardix, S.; Steinberger, I. T. The Mechanism of Polytype Formation in Vapour-Phase Grown ZnS Crystals. *Philos. Mag.* **1970**, *21*, 1237–1246.
42. Suzuki, K.; Ichihara, M.; Takeuchi, S. High-Resolution Electron-Microscopy of Extended Defects in Wurtzite Crystals. *Jpn. J. Appl. Phys. 1* **1994**, *33*, 1114–1120.
43. Stampfl, C.; Van de Walle, C. G. Energetics and Electronic Structure of Stacking Faults in AlN, GaN, and InN. *Phys. Rev. B* **1998**, *57*, 15052–15055.
44. Blank, H.; Delavignette, P.; Gevers, R.; Amelinckx, S. Fault Structures in Wurtzite. *Phys. Status Solidi* **1964**, *7*, 747–764.
45. Komninou, P.; Kioseoglou, J.; Dimitrakopulos, G. P.; Kehagias, T.; Karakostas, T. Partial Dislocations in Wurtzite GaN. *Phys. Status Solidi A* **2005**, *202*, 2888–2899.
46. Ding, Y.; Kong, X. Y.; Wang, Z. L. Doping and Planar Defects in the Formation of Single-Crystal ZnO Nanorings. *Phys. Rev. B* **2004**, *70*, 235408.
47. Jin, L.; Wang, J. B.; Choy, W. C. H. Growth of ZnSe Nanospirals with Bending Mediated by Lomer-Cottrell Sessile Dislocations through Varying Pressure. *Cryst. Growth Des.* **2008**, *8*, 3829–3833.
48. Jin, L.; Wang, J. B.; Jia, S. F.; Jiang, Q. K.; Yan, X.; Lu, P.; Cai, Y.; Deng, L. Z.; Choy, W. C. H. ZnSe Heterocrystalline Junctions Based on Zinc Blende-Wurtzite Polytypism. *J. Phys. Chem. C* **2010**, *114*, 1411–1415.
49. Frank, F. C. Capillary Equilibria of Dislocated Crystals. *Acta Crystallogr.* **1951**, *4*, 497–501.
50. Heindl, J.; Strunk, H. P.; Heydemann, V. D.; Pensl, G. Micropipes: Hollow tubes in silicon carbide. *Phys. Stat. Sol. A* **1997**, *162*, 251–262.
51. Morin, S. A.; Bierman, M. J.; Tong, J.; Jin, S. Mechanism and Kinetics of Spontaneous Nanotube Growth Driven By Screw Dislocations. *Science* **2010**, *328*, 476–480.
52. Hacialioglu, S.; Meng, F.; Jin, S. Facile and Mild Solution Synthesis of Cu_2O Nanowires and Nanotubes Driven by Screw Dislocations. *Chem. Commun.* **2012**, *48*, 1174–1176.
53. Maestre, D.; Haeussler, D.; Cremades, A.; Jaeger, W.; Piqueras, J. Nanopipes in In_2O_3 Nanorods Grown by a Thermal Treatment. *Cryst. Growth Des.* **2011**, *11*, 1117–1121.
54. Maestre, D.; Haussler, D.; Cremades, A.; Jager, W.; Piqueras, J. Complex Defect Structure in the Core of Sn-Doped In_2O_3 Nanorods and Its Relationship with a Dislocation-Driven Growth Mechanism. *J. Phys. Chem. C* **2011**, *115*, 18083–18087.
55. Duan, J. H.; Yang, S. G.; Liu, H. W.; Gong, J. F.; Huang, H. B.; Zhao, X. N.; Zhang, R.; Du, Y. W. Preparation and Characterization of Straight and Zigzag AlN Nanowires. *J. Phys. Chem. B* **2005**, *109*, 3701–3703.
56. Wang, H.; Liu, G.; Yang, W.; Lin, L.; Xie, Z.; Fang, J. Y.; An, L. Bicrystal AlN Zigzag Nanowires. *J. Phys. Chem. C* **2007**, *111*, 17169–17172.
57. Ross, F. M. Controlling Nanowire Structures through Real Time Growth Studies. *Rep. Prog. Phys.* **2010**, *73*, 114501.
58. Jacobs, B. W.; Crimp, M. A.; McElroy, K.; Ayres, V. M. Nanopipes in Gallium Nitride Nanowires and Rods. *Nano Lett.* **2008**, *8*, 4353–4358.
59. Luo, S. D.; Zhou, W. Y.; Wang, W. X.; Zhang, Z. X.; Liu, L. F.; Dou, X. Y.; Wang, J. X.; Zhao, X. W.; Liu, D. F.; Gao, Y.; *et al.* Template-free Synthesis of Helical Hexagonal Microtubes of Indium Nitride. *App. Phys. Lett.* **2005**, *87*, 063109.
60. Tizei, L. H. G.; Craven, A. J.; Zagonel, L. F.; Tence, M.; Stephan, O.; Chiaramonte, T.; Cotta, M. A.; Ugarte, D. Enhanced Eshelby Twist on Thin Wurtzite InP Nanowires and Measurement of Local Crystal Rotation. *Phys. Rev. Lett.* **2011**, *107*, 195503.
61. Forticaux, A.; Hacialioglu, S.; Degrave, J. P.; Dziedzic, R.; Jin, S. Three-Dimensional Mesoscale Heterostructures of ZnO Nanowire Arrays Epitaxially Grown on $CuGaO_2$ Nanoplates as Individual Diodes. *ACS Nano* **2013**, *7*, 8224–8232.
62. Cheze, C.; Geelhaar, L.; Brandt, O.; Weber, W. M.; Riechert, H.; Munch, S.; Rothemund, R.; Reitzenstein, S.; Forchel, A.; Kehagias, T.; *et al.* Direct Comparison of Catalyst-free and Catalyst-Induced GaN Nanowires. *Nano Res.* **2010**, *3*, 528–536.
63. Arbiol, J.; Estrade, S.; Prades, J. D.; Cirera, A.; Furtmayr, F.; Stark, C.; Laufer, A.; Stutzmann, M.; Eickhoff, M.; Gass, M. H.; *et al.* Triple-Twin Domains in Mg Doped GaN Wurtzite Nanowires: Structural and Electronic Properties of This Zinc-Blende-like Stacking. *Nanotechnology* **2009**, *20*, 145704.